VAASAN AMMATTIKORKEAKOULU
UNIVERSITY OF APPLIED SCIENCES

Minh Nguyen

BLDC MOTOR PID CONTROLER

Technology and Communication
2021

VAASAN AMMATTIKORKEAKOULU
UNIVERSITY OF APPLIED SCIENCES
Information Technology

ABSTRACT

Author	Minh Nguyen
Title	BLDC Motor PID Controller
Language	English
Pages	41 + 3 Appendices
Name of Supervisor	Jani Ahvonen

The brushless DC motors have an unlimited number of applications nowadays, many of which require the motor speeds to be controlled. The PID controllers is the answer for the mentioned problem. This project implemented a PID algorithm to regulate a brushless DC motor speed using a programmed microcontroller unit.

In this project, a NUCLEO-152RE development board was used as a controller unit and a X-NUCLEO-IHM07M1 expansion board served as a motor driver and power unit. The selected BLDC motor was the Nanotec DF45M024053-A2 model coming with the hall-effect sensors. This project was built based on C Embedded Project using Atollic TrueSTUDIO 9.3.0 IDE. It implemented a six-step algorithm serving the purpose of driving the BLDC motor and PID algorithm to control the motor speed.

The results yielded showed that the PID controller eliminated the need of manual control (by human) but slightly decreased the system stability. The impact of PID controller also decreased with an increasing target speed value due to the maximum angular acceleration of the motor.

Keywords Brushless, DC, motor, PID, controller

TABLE OF CONTENTS

LIST OF ABBREVIATIONS

BLDC	Brushless Direct Current
CD	Compact Disk
CMSIS	Cortex Microcontroller Software Interface Standard
DC	Direct Current
GPIO	General Pin Input/Output
IDE	Integrated Development Environment
LED	Light-Emitting Diode
PID	Proportional-Integral-Derivative
PV	Process Variable
PWM	Pulse-Width Modulation
RCC	Reset and Clock Control
SP	Setpoint

LIST OF FIGURES AND TABLES

LIST OF APPENDICES

1 INTRODUCTION

In today's world, brushless direct current (BLDC) motors can be found in many applications ranging from big propulsion systems in an electric aircraft to a small compact disk (CD) drive. For some cases, it is critical for the motor speed to be controlled which leads to the need of motor controllers.

The proportional-integral-derivative controllers (PID controllers) apply a control mechanism using proportional, integral and derivative terms to calculate optimal outputs from the differences between the measured values and the target value /3/. The PID concept is the most used control algorithm in industrial control systems because of its superior precision and accuracy.

The PID controller is a solution to the mentioned problem. This project aimed to implement the PID controller algorithm on an ARM microcontroller to regulate a BLDC motor speed.

2 LITERARY REVIEW

In this section of the thesis, the theoretical ideas behind the project are explained. There are two fundamental theory parts that are the **DC motor** and the **PID controller**.

2.1 DC Motor

A DC motor generally transform electrical energy to mechanical energy in form of rotation /1/. The stationary part called **stator** and the moving part called **rotor** of a DC motor consist of permanent magnets or electromagnets (made by running the current through the solenoids) which generate magnetic fields. The attractive force between two magnetic fields made the motor rotate as illustrated in **Figure 1**.

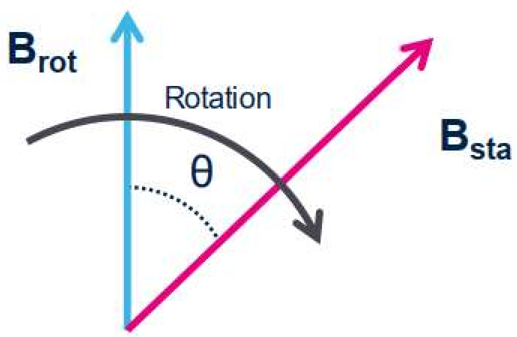

Figure 1. The working principle behind the rotation of DC motor /9/

The formula for the torque applied on the rotor is given below.

$$\tau \propto B_{\mathrm{rot}} \cdot B_{\mathrm{sta}} \cdot \sin(\theta) \qquad (1)\ /9/$$

where

- τ is the torque
- B_{rot} is the magnetic fields generated by the rotor
- B_{sta} is the magnetic fields generated by the stator

- θ is load angle (the angle between two vectors $\overrightarrow{B_{\mathrm{rot}}}$ and $\overrightarrow{B_{\mathrm{sta}}}$)

Deduced from the formula, the maximum output torque is archived with the load angle θ being 90°.

There are two common types of DC motor which are brushed and brushless ones.

2.1.1 Brushed DC Motor

In a brushed DC motor, the rotor is composed of pairs of solenoids and the stator consists of permanent magnets. The stator electromagnetic field remains fixed while the rotor electromagnetic field is constantly changing during the rotation. The load angle is kept close to 90° by constantly charging the next pair of solenoids when they come to a specific position (as in **Figure 2**).

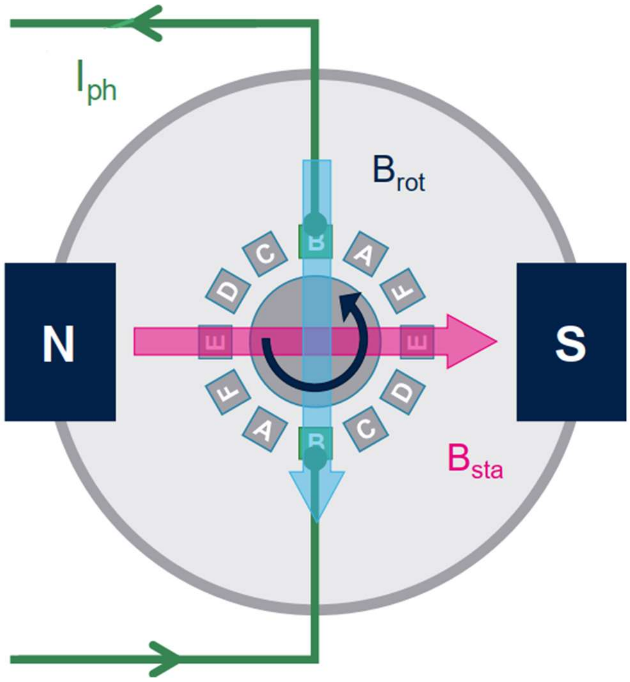

Figure 2. Working principle of brushed DC motor /20/

The connectors between the circuit and solenoids are called brushes, thus the name of brushed DC motor. Changing the current the direction will make the motor to rotate in the opposite direction.

2.1.2 Brushless DC Motor

A brushless DC motor has the rotor containing a permanent magnet and its stator consists of three solenoids connected in a star topology and positioned 120° from each other. The rotor electromagnetic field changes with the rotation so that in order to keep the load angle as close to 90° as possible, the stator electromagnetic field is constantly changed according to the position of the rotor. **Figure 3** below show the structure and working principle of a brushless DC motor.

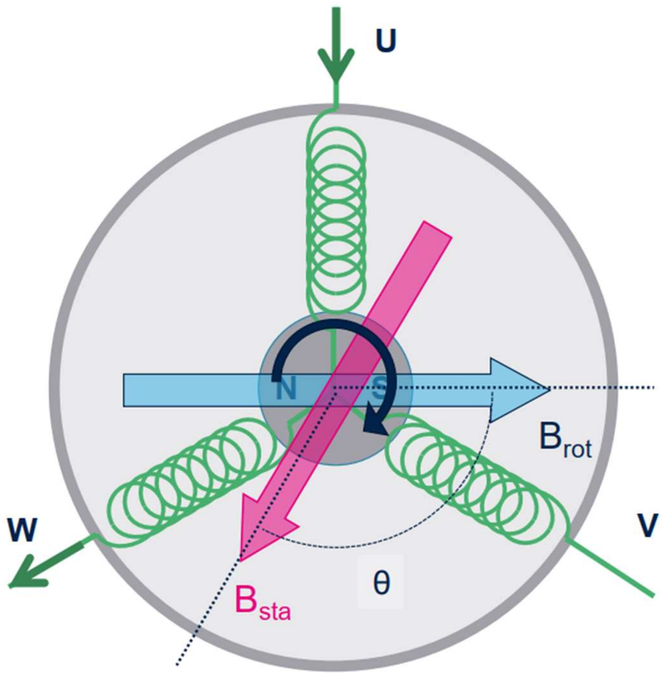

Figure 3. Physical structure and working principle of brushless DC motor /11/

Even though brushed DC motors have a low initial cost and simple control of motor speed, the high maintenance of the brushes makes the brushless counterpart superior in terms of durability and reliability. However, operating a brushless DC motors is more complex.

Brushless motors can be constructed in several different physical configurations: In the 'conventional' (also known as inrunner) configuration, the permanent magnets are part of the rotor. Three stator windings surround the rotor. In the outrunner (or external-rotor) configuration, the radial-relationship between the coils and magnets is reversed; the stator coils form the centre (core) of the motor, while the permanent magnets spin within an overhanging rotor which surrounds the core. /2/

2.1.3 Six-step Algorithm

The six-step algorithm is a driving operation of three-phase BLDC motors. In six-step, there are six current directions running through two of the three phases, which created six discrete directions of magnetic field for the stator (illustrated in **Figure 4**). To acquire the position of the rotor, the hall-effect sensors are used for sensored BLDC motors and BEMF feedbacks are used for the sensorless counterparts. Eventually, the correct step is applied accordingly to the known rotor position and the intended rotation direction.

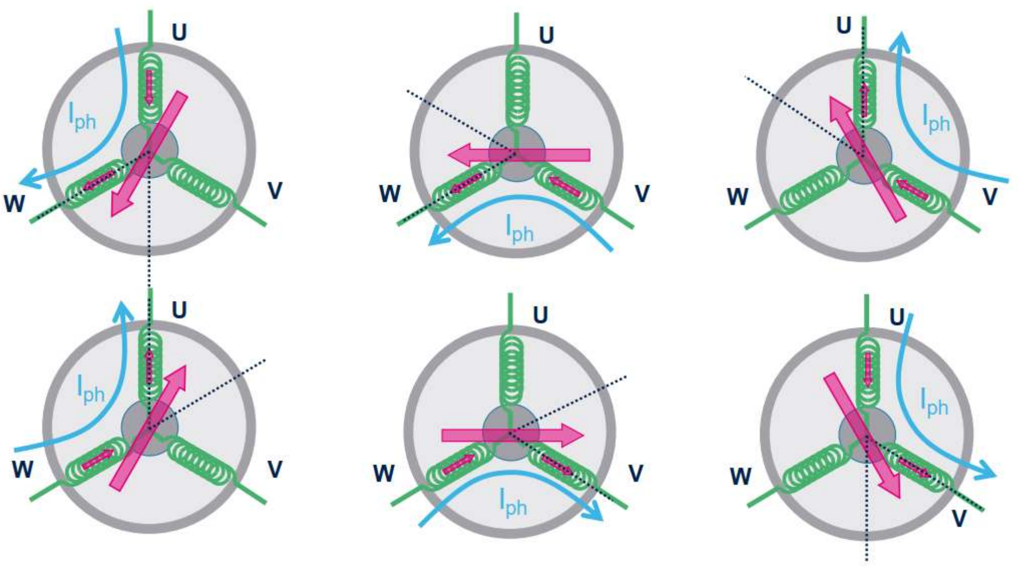

Figure 4. Six combinations in six-step algorithm /12/

2.2 PID Controller

A **proportional-integral-derivative controller** (also known as a PID controller or three-term controller) is a closed loop control mechanism that is widely used in industrial control systems. It uses the three control terms of proportional, integral and derivative to calculate the output from the error value, which is the difference between the designated target value called a setpoint (SP) and the measured feed-back value called a process variable (PV). /3/

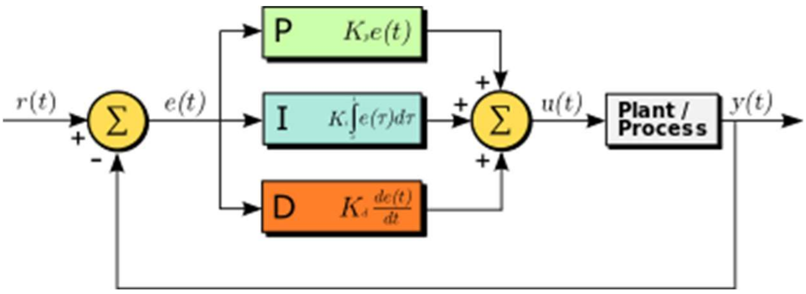

Figure 5. The working principle of PID controller /3/

The mathematical formula of overall control function of PID controller is

$$u(t) = K_p \cdot e(t) + K_i \cdot \int_0^t e(\tau)d\tau + K_d \cdot \frac{de(t)}{dt} \qquad (2)\ /3/$$

where

- t is running time
- τ is integral time
- $r(t)$ is setpoint
- $e(t)$ is error
- $u(t)$ is control variable
- $y(t)$ is process variable
- K_p is proportional gain
- K_i is integral gain
- K_d is derivative gain

From the block diagram in **Figure 5**, the error value $e(t)$ as a difference between setpoint $r(t)$ and process variable $y(t)$ is continuously measured then the output control variable $u(t)$ is calculated based on proportional, integral and derivative terms to minimize the error over time. /3/

Even though the PID controller has three control terms, some applications may not need all of them to have appropriate control. In those cases, the selective use of the control terms can be achieved by setting the coefficients (K_p, K_i or K_d) of unnecessary terms to 0 so that they have no impact on the output. /3/

2.2.1 Proportional Term

The proportional term produces an output value that is proportional to the error value. The P term takes the formula

$$P = K_p \cdot e(t) \quad (3)$$ /3/

By changing the coefficient K_p (also known as proportional gain), the response of output based on P term can be adjusted. If the proportional gain is too large, the system overreacts with the error value and the process variable oscillates around the setpoint, which increases the settling time and decreases the stability. Meanwhile, with small proportional gain, the system becomes less responsive, and the rise time is increased. /3/

Figure 6 below shows the graph of process variable responses with different values of K_p.

The proportional term alone cannot correct the system of steady-state error, which is the difference between the desired final output and the actual one. /3/

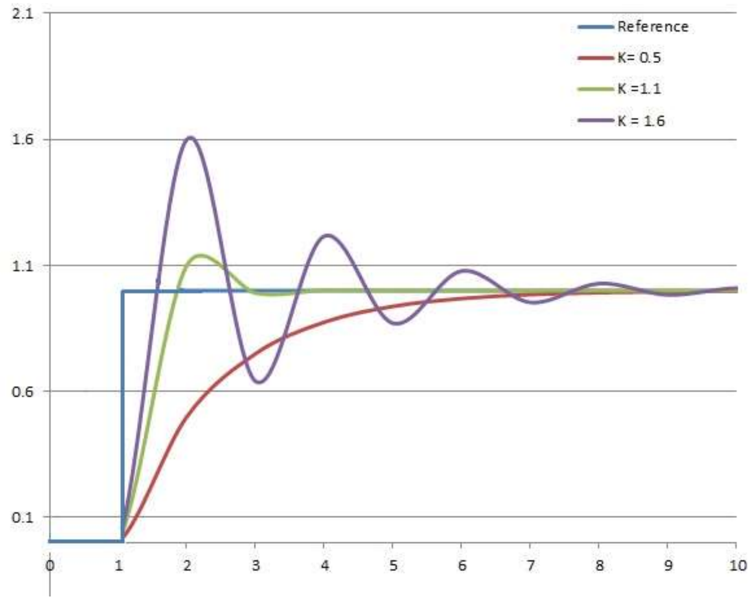

Figure 6. System responses with different value of K_p /3/

2.2.2 Integral Term

The integral term considers both the error and the duration of the error when calculating an output /3/. In fact, the mathematical formula for I term comes with the integral, which is the sum of instantaneous errors over time.

$$I = K_i \cdot \int_0^t e(\tau)d\tau \qquad (4)\ /3/$$

Increasing the K_i gain to, thus increasing the impact of I term, will help to eliminate the steady-state error but in exchange it increases the overshoot, settling time and decreasing system stability /3/. The graph in **Figure 7** illustrates how I term affects the system respond.

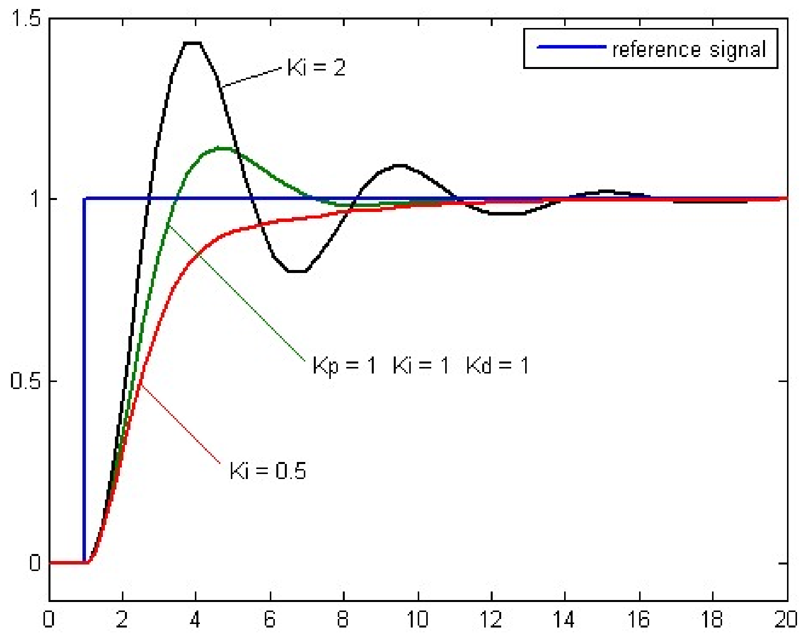

Figure 7. System responses with different value of K_i /3/

2.2.3 Derivative Term

The derivative term produces an output base on the derivative of the errors, in other words, it takes into calculation the error change rate over time /3/. The mathematical formula for the derivative term is

$$D = K_d \cdot \frac{de(t)}{dt} \qquad (5)\ /3/$$

By predicting the error changes in the system, the derivative term largely decreases the settling time while improving the stability with small K_d value /3/. The graph in **Figure 8** shows the system response with different value of K_d.

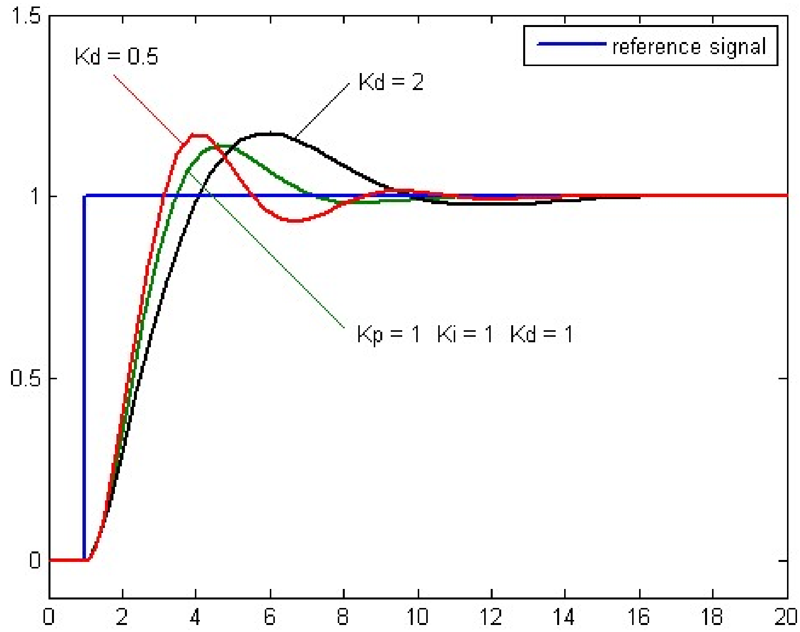

Figure 8. System responses with different value of K_d /3/

2.2.4 Tuning

Different control systems have different control parameter values that lead to their desired control responses and the work of finding those optimal values is called **tuning**. The system requirements may include the rise time, settling time, overshoot allowance but the basic one is stability /3/. There are various tuning methods with different levels of sophistication but in this project, manual tuning method was used.

Manual tuning requires understanding the impact on the system of control terms and adjusting them one by one (firstly K_p, then K_i and finally K_d) until the system response meets the requirements.

3 METHODS

In this section, the resources used for the project are listed and the conducting method, as well as the measuring results, are interpreted.

3.1 Resources

The resource consumed, apart from working hours and materials, can be divided into two parts: **hardware** and **software**.

3.1.1 Hardware

The hardware selected for the project consisted of a **NUCLEO-L152RE** development board serving as a controller, a **X-NUCLEO-IHM07M1** expansion board serving as a power block and a Nanotec **DF45M024053-A2** sensored BLDC motor. The **Figure 9** below shows the theoretical layer structure of the hardware.

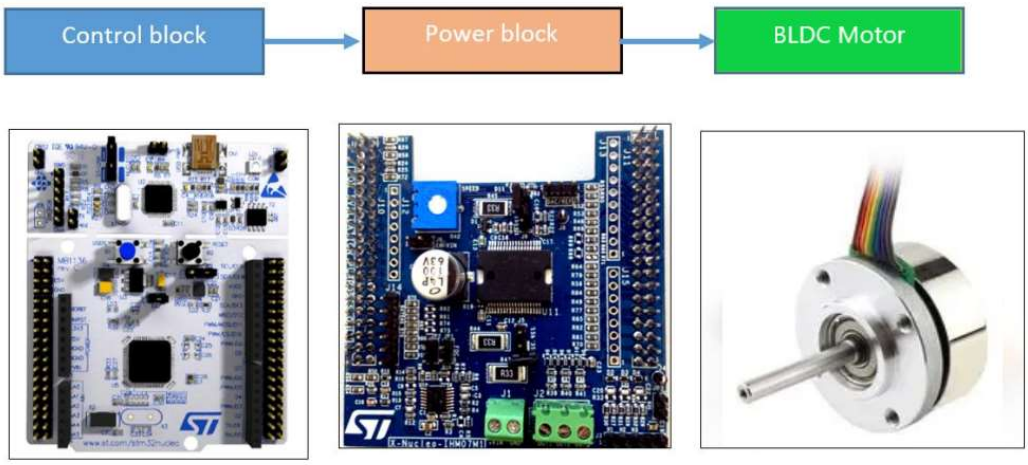

Figure 9. The hardware structure of the project /7/

The NUCLEO-L152RE belongs to the STM32 Nucleo-64 board family which is produced by STMicroelectronics. It features the STM32 microcontrollers with the 32-bit ARM processor core which are widely used in real-life embedded system applications. This development board is also an affordable and flexible device to study, try out new concepts and build prototypes, thus, it suited for this project /4/.

The X-NUCLEO-IHM07M1 is a three-phase brushless DC motor driver expansion board based on the L6230 for STM32 Nucleo. It is produced by the same manufacturer, STMicroelectronics, to provide an affordable and easy-to-use solution for driving a three-phase brushless DC motor /5/.

The brushless DC motor model DF45M024053-A2 is produced by Nanotec Electronic GmbH & Co. KG. It is a 12N16P outrunner type which contains 16 poles of permanent magnet in the outer rotor and 12 coils connected to 3 current phases, serving as stator electromagnets.

Apart of the main hardware, an oscilloscope was used to measure motor speed changes.

3.1.2 Software

Atollic TrueSTUDIO 9.3.0 was used during the coding part of this project. Atollic TrueSTUDIO is an Eclipse based IDE that is commercially enhanced by STMicroelectronics. It provides extension, features and utilities that support devices produced by the same manufacturer, thus, are highly suitable to work with NUCLEO-L152RE /6/.

The project was based on the C Embedded Project template provided by TrueSTUDIO, which contains Cortex Microcontroller Software Interface Standard library (CMSIS) serving as a foundation of the project software.

3.2 System Building

The X-NUCLEO-IHM07M1 was connected to the NUCLEO-L152RE development board through an ST-morpho connector, and its jumper configuration was left default as in **Table 1**. The motor was connected to the expansion board following **Table 2** below. The external DC voltage is connected to J1 section of the board.

The circuit diagrams of the D6230 three-phase BLDC motor driver and hall/encoder sensors are displayed in **APPENDIX 2** and **3**. **Figure 10** below shows the complete configuration of the system hardware.

Table 1. X-NUCLEO-IHM07M1 Jumper settings /8/

Jumper	Permitted configurations	Default condition
JP1	Selection for pull-up insertion (BIAS) in current sensing circuit	OPEN
JP2	Selection for op amp gain modification in current sensing circuit	OPEN
JP3	Selection for pull-up enabling in Hall/Encoder detection circuit	CLOSED
J9	Selection to supply the STM32 Nucleo board through the X-NUCLEOIHM07M	OPEN
J5	Selection for single/three shunt configuration. Set to single shunt by default	2-3 CLOSED
J6	Selection for single/three shunt configuration. Set to single shunt by default	2-3 CLOSED
J7	Debug connector for DAC. Available for probe connection	OPEN

Table 2. Motor and IHM07M1 pin matching

X-NUCLEO-IHM07M1		DF45M024053-A2
J3	GND	GND
	5V	VCC
	A+	H1
	B+	H2
	Z+	H3
J2	OUT3	PHW
	OUT1	PHU
	OUT2	PHV

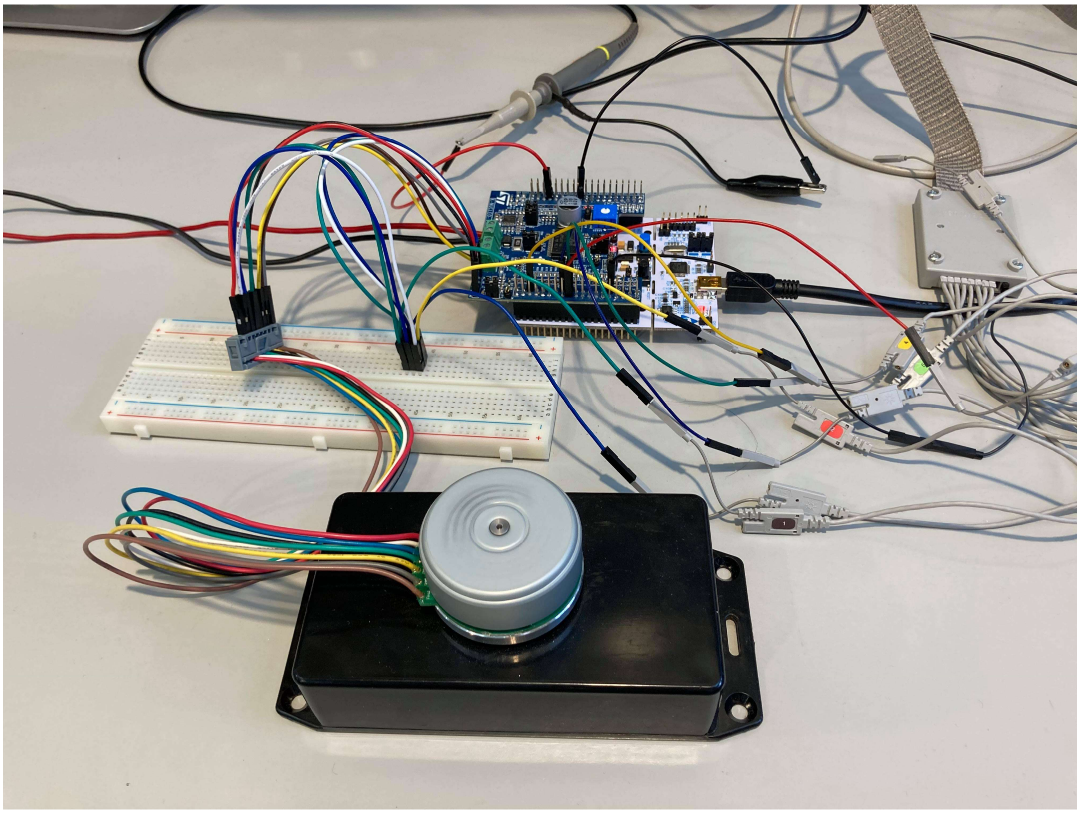

Figure 10. System hardware

3.3 Programming

The program starts with the initialisation of PID controller by setting PID parameters and a target speed which will remain constant during the runtime. It then calculates an optimal value for PWM duty cycle using the PID algorithm and the error between the target speed and the motor speed. In the next steps, the program reads the motor position (or current step in six-step algorithm), enables and generates PWM to the correct channels, which will then make the motor run. These steps will run indefinitely if there is no external interrupt caused by a hall sensor signal. If an interrupt is triggered, marking one eighth of revolution was done, the motor value would be calculated based on the timer value. Finally, a new PWM duty cycle value is calculated using the newly measured motor speed and the program continues. The main logic of the program is illustrated by the flow diagram in **Figure 11**.

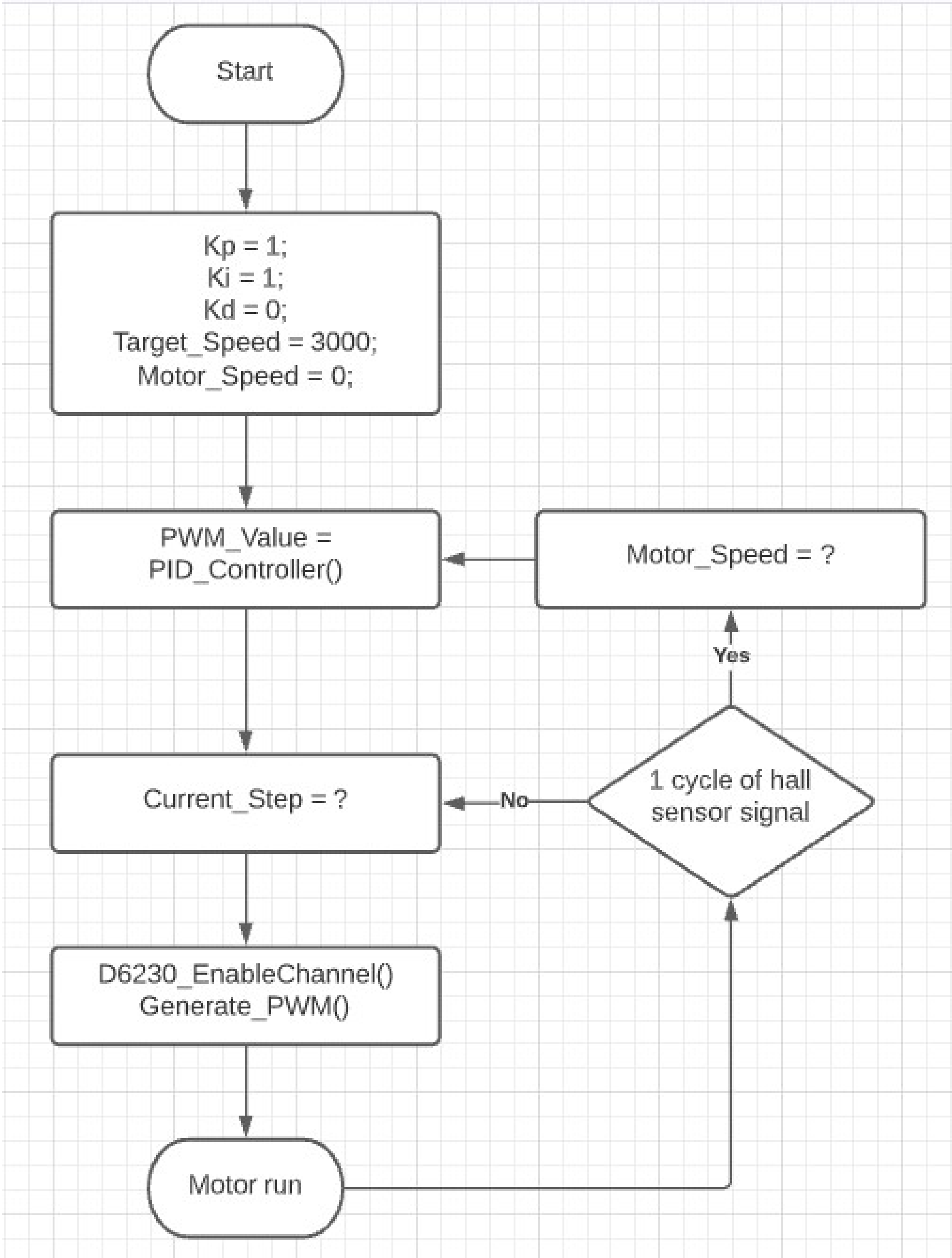

Figure 11. Program logic flow diagram

The project was built based on a C Embedded Project template that is specifically designed for NUCLEO-L152RE and provided by Atollic TrueSTUDIO IDE. The project was given the name **BLDC_Motor_PID_Controller**. The **Figure 12** below illustrates the structure of the program.

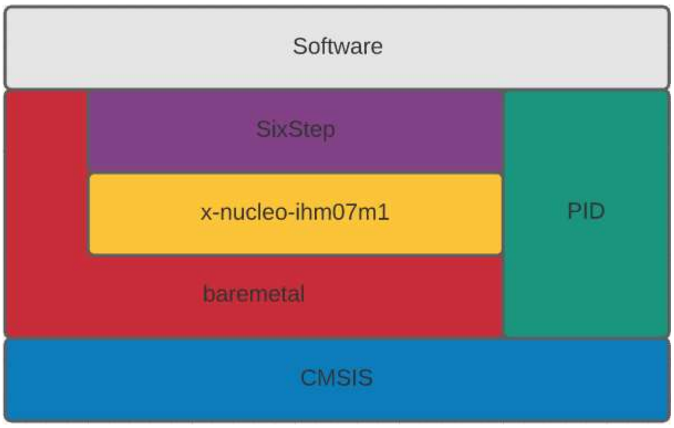

Figure 12. Program layer structure

In the program structure, the bottom layer called CMSIS was provided by the project template, serving as the foundation of the program. The remaining parts were developed by the author of this project in separated C source code and header files.

3.3.1 Baremetal Files

"Baremetal" files were the first to be written which contain functions executing bit operations directly to registers and can be called in upper layers to do basic specific tasks. These files are independent from each other to ensure their modularity and reusability. In this project, the following sections had baremetal files:

- Reset and clock control (RCC)
- General-purpose input/output (GPIO)
- Timers (TIM)

3.3.2 Device-specific Files

Files "x-nucleo-ihm07m1.c" and "x-nucleo-ihm07m1.h" served as a driver for the X-NUCLEO-IHM07M1 expansion board, which contained functions to use the D6230 three-phase motor driver, the hall-effect sensor encoder and the debug LED.

For the same purpose, “nucleo-l152re.c” and “nucleo-l152re.h” were created specifically for the NUCLEO-L152RE board and they contained only functions to control the user LED.

3.3.3 Six-step Algorithm

The six-step algorithm was implemented in “SixStep.c” and “SixStep.h”. These files contained functions to execute the specific tasks which are

- Generating pulse-width modulation (PWM) to 3 channels of the D6230 three-phase motor driver.
- Reading the hall-effect sensor to determine at which step the motor is.
- Measuring the motor speed based on the time between different consecutive steps.

The “SixStep” files were created specifically for the X-NUCLEO-IHM07M1 board and the Nanotec DF45M024053-A2 sensored motor. They were not written as a general six-step driver and cannot used for other hardware because of the following reasons

- Functions in X-NUCLEO-IHM07M1 driver were called directly in SixStep functions.
- Six-step table were based on the hall-effect sensor reading function and wiring diagram in the DF45M024053-A2 datasheet.

Because of its specific target, it is unnecessary to write functions that implement the six-step algorithm based on BEMF feedbacks, thus, there are no option for a sensorless motor.

3.3.4 PID Controller

The PID module contained "PID.c and PID.h" and was built as a standalone module for the purpose of reusability. In this module, the PID algorithm was implement based on the pseudocode in **Figure 13** below.

```
previous_error := 0
integral := 0

loop:
    error := setpoint − measured_value
    integral := integral + error × dt
    derivative := (error − previous_error) / dt
    output := Kp × error + Ki × integral + Kd × derivative
    previous_error := error
    wait(dt)
    goto loop
```

Figure 13. Pseudocode for PID algorithm

As seen in Figure 13, the `error` is the different between the `setpoint` and the `measured_value` (or feedback value). The ways integral and derivative are calculated in the code

```
integral := integral + error * dt

derivative := (error − previous_error) / dt
```

reflect the mathematical formulas (4) and (5) above.

The `dt` in the pseudocode is the time between each time the code inside the loop is executed, which can also be understood as a sample period of the implemented PID controller. In this project, the time between samples was implemented to be a constant during the whole operation, thus, `dt` in the formulas was merged with `Ki` and `Kd` constants.

3.3.5 Main Software

The main.c file contained the main part of the program which is also considered to be the software layer. The block diagram in **Figure 14** shows how the PID controller and BLDC were implemented in this project software.

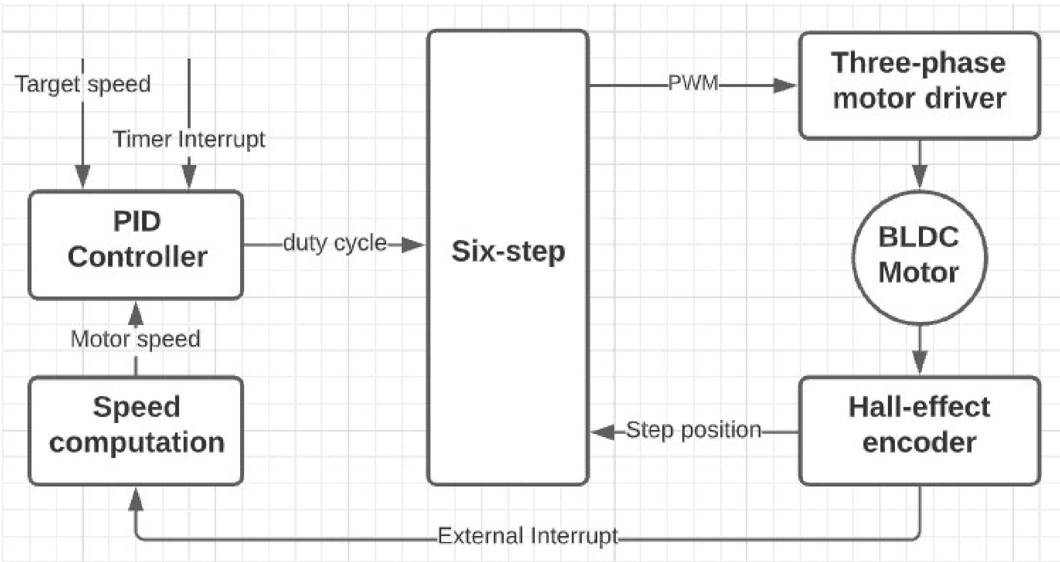

Figure 14. Implementation block diagram

The main function started with setting up and enabling all necessary interrupt routine service (IRQ) and the initialisations of the SixStep algorithm and PID controller. PID parameters, such as setpoint, term gains, upper and lower output limits were input using the `PID_Init()` function. After the initialisations and the one-time-run code, the following parts run continuously during the whole operation.

- The six-step functions generating PWM pulses and reading the current step of the motor was placed in the `while(1)` loop of the main function.
- PID controller function calculating the output as the PWM duty cycle was called by the timer interrupt handler (`TIM7_IRQHandler()`) generated with 1 kHz frequency.
- Speed computation was performed every time the hall-sensor signal triggered external interrupt (`EXTI15_10_IRQHandler()`).

3.4 Measuring

After success in compiling and downloading the source code to the microcontroller, multiple measurements were performed to reveal the internal operation of the system in various situations, with and without PID controller.

3.4.1 Motor Driving Operation

The first test runs were performed to see how the system worked during the six-step algorithm, in which the hall sensor signal (A+/H1, B+/H2 and Z+/H3 in **APPENDIX 3**) and PWM signals (IN1, IN2 and IN3 in **APPENDIX 2**) were captured using the digital probe of the oscilloscope. The PID controller was not initialised during these tests. **Figure 14** below shows the measurement at PWM value equal 2500, in which

- D_0 measured Encoder A/Hall H1 at PA15
- D_1 measured Encoder B/Hall H2 at PB3
- D_2 measured Encoder Z/Hall H3 at PB10
- D_3 measured UH_PWM at PA8
- D_4 measured VH_PWM at PA9
- D_5 measured WH_PWM at PA10

The motor speed could be calculated using the frequency of any hall signal and the formula below:

$$\text{motor\_speed} = \frac{f_{D_0}}{8} \times 60 = \frac{218.61}{8} \times 60 \approx 1640 \text{ RPM}$$

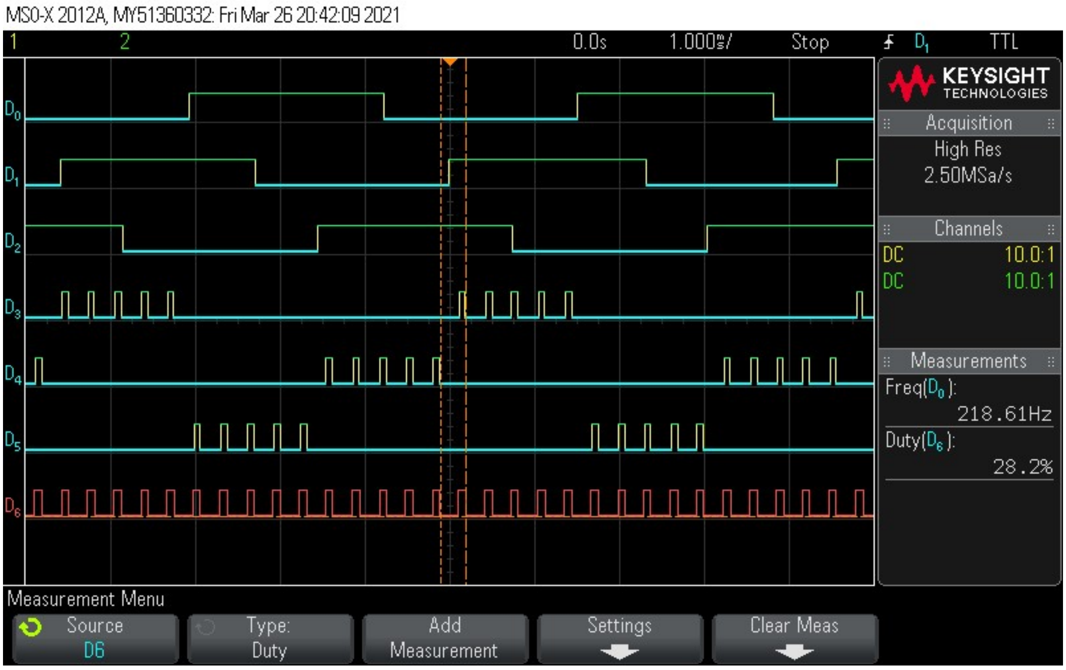

Figure 15. Hall sensor and PWM signals in six-step algorithm

The performance and responses of the motor with various PWM values were also measured, captured and calculated. During these tests, the pulse value was manually set and incremented starting from 0 to 10000 with the step of 500. The frequency of the hall sensor H1 measured by the oscilloscope and average motor speed calculated are displayed in **Table 2** below. For each PWM value, 8 samples of frequency and speed were recorded and calculated. The full measurement data are displayed in **APPENDIX 1**.

Table 3. Motor speeds at different PWM values

PWM value	average frequency	average speed	error
0	0.0	0	0
500	34.7	261	8
1000	60.1	451	7
1500	113.4	851	6
2000	175.2	1314	11
2500	216.6	1624	12

3000	254.1	1905	12
3500	291.1	2183	11
4000	345.0	2587	21
4500	394.1	2956	17
5000	457.7	3433	18
5500	484.8	3636	24
6000	532.4	3993	33
6500	589.5	4422	21
7000	627.4	4705	30
7500	672.1	5041	37
8000	710.3	5327	35
8500	750.4	5628	32
9000	799.3	5995	27
9500	877.3	6580	37
10000	915.5	6866	33

3.4.2 The Impact of PID controller

In these measurements, test runs were performed to tune the parameters of the PID controller. The control terms proportional and integral were selected, and derivative term was disabled as in most real-life control systems. The PI controller was **manually tuned** by the following steps:

- Setting a small K_p value (preferably $\frac{\text{maximum PWM value}}{\text{maximum motor speed}}$) and K_i equal 0.
- Adding small K_i (preferably $\frac{K_p}{\text{PID sample rate}}$) so that the system can correct the steady-state error.
- Manually increasing K_i to the maximum value that did not cause an overshoot.
- Increasing K_p so that the rise time was improved.

- Repeat the two previous steps until the rise time and settling time improvement was minor.

Figures 15, 16, 17 and **18** below show the system responses with different value of K_i during tuning. The motor speed changes were the analog output of DAC module channel 1, pin PA4 and were captured with probe 1 of the oscilloscope.

After tuning the PID controller, three target speed values were selected to test how effective it was at different speed ranges. The oscilloscope pictures (from **Figure 19** to **Figure 30**) with the measurements displayed in the order to show the system rise time then settling time, with the PID, then without the PID and from small to large target speed values. The measurement results are also displayed in **Table 4** below.

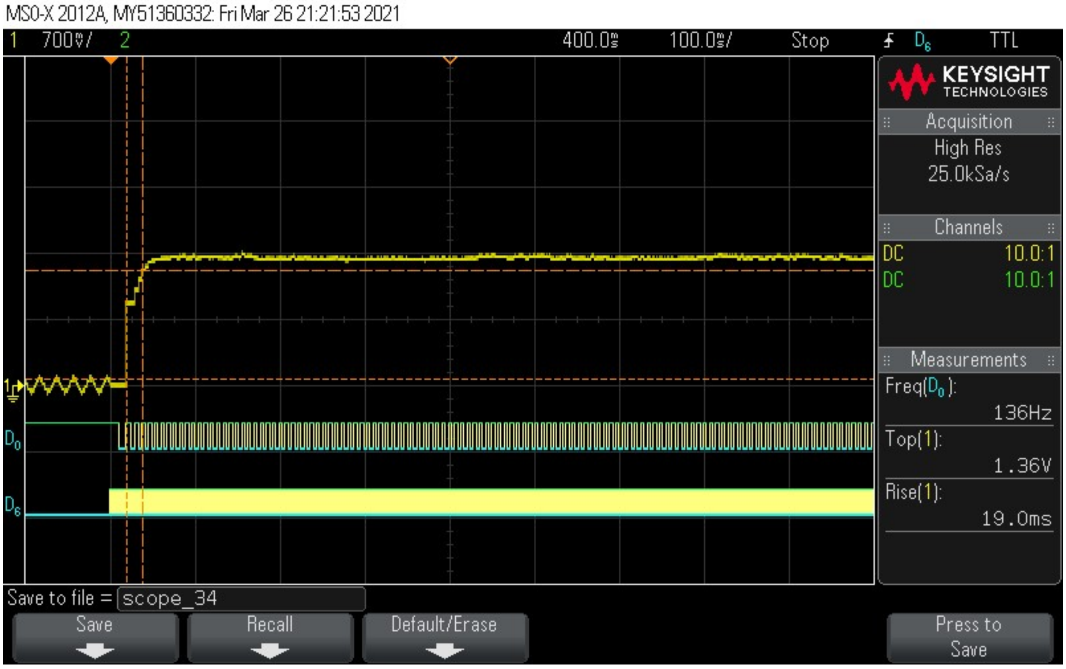

Figure 16. Steady-state error with K_p alone

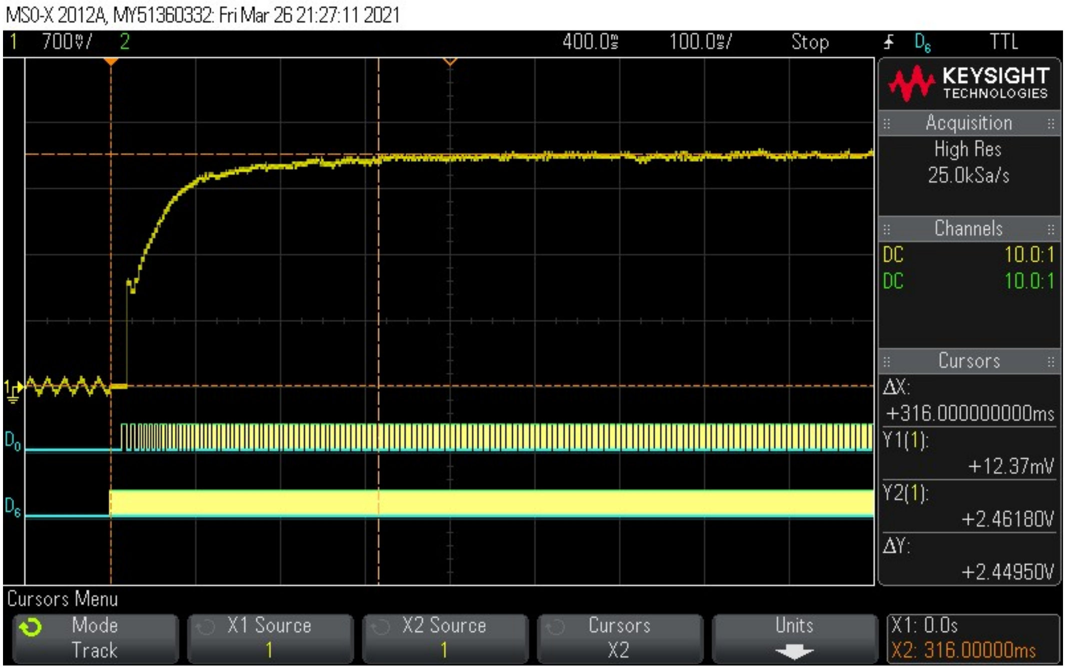

Figure 17. Long settling time with small K_i

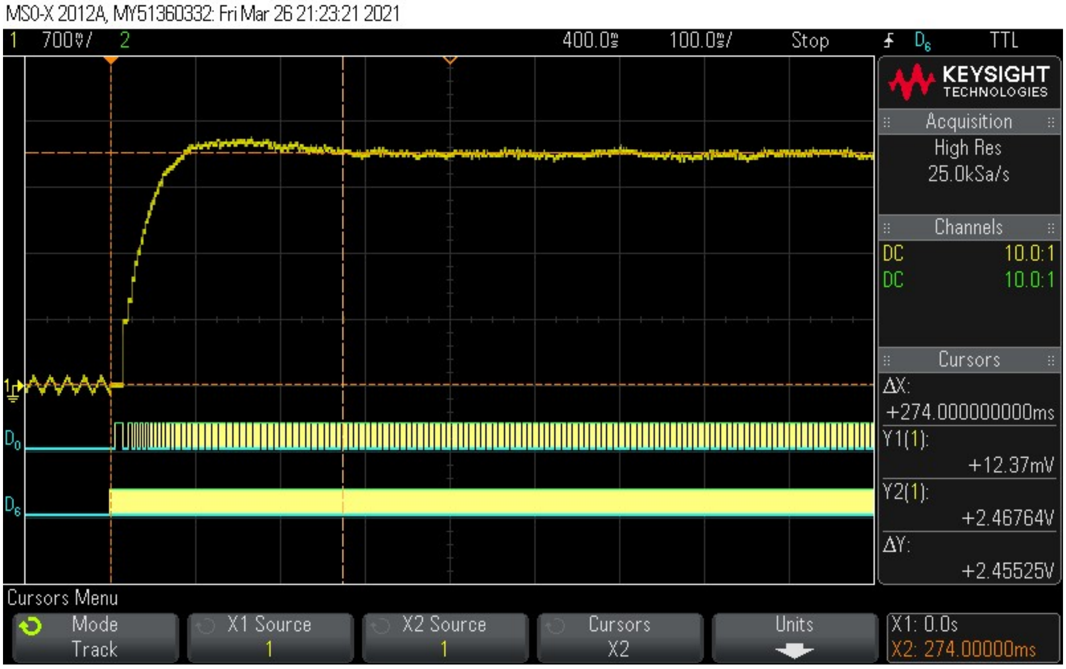

Figure 18. Overshoot happened with larger value of K_i

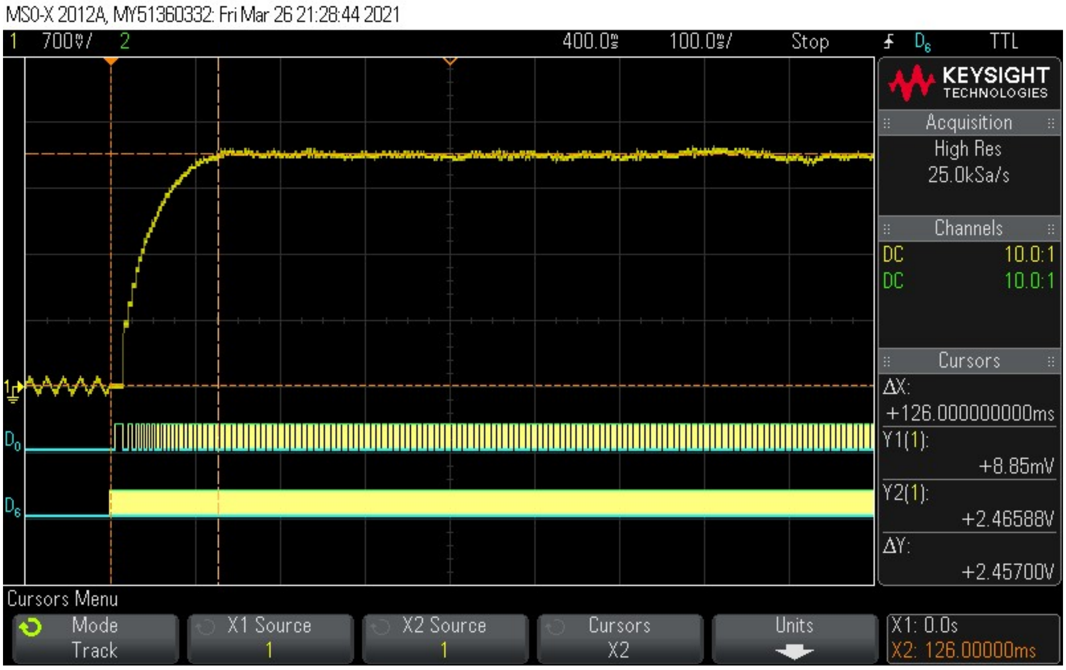

Figure 19. Perfect system response with K_i being optimal to current K_p

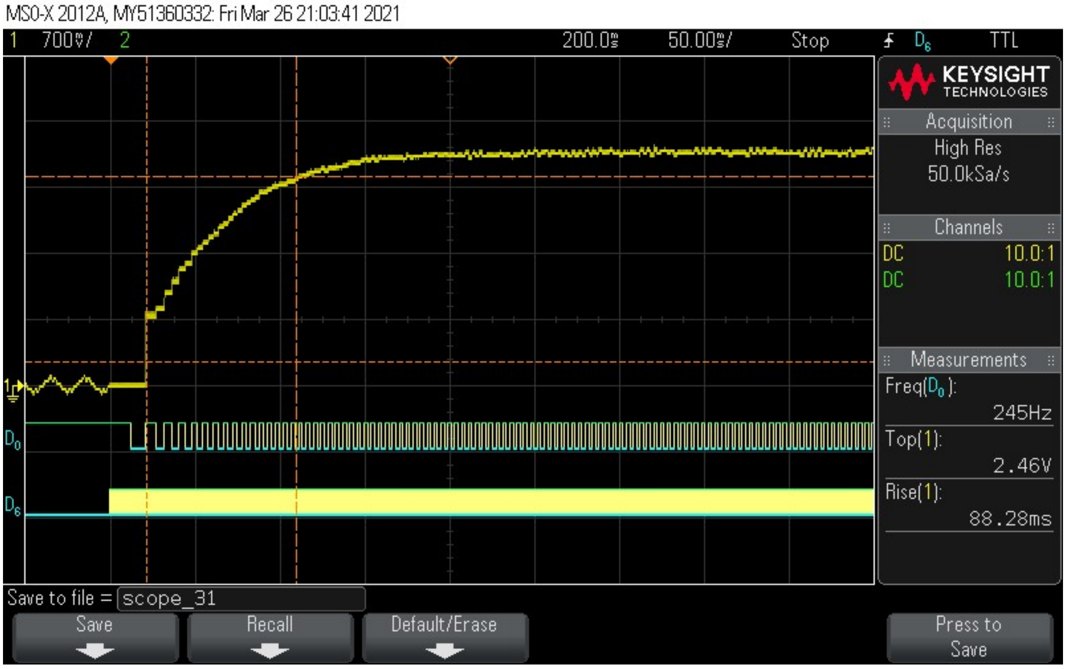

Figure 20. System rise time without PID at target speed of 1850 RPM

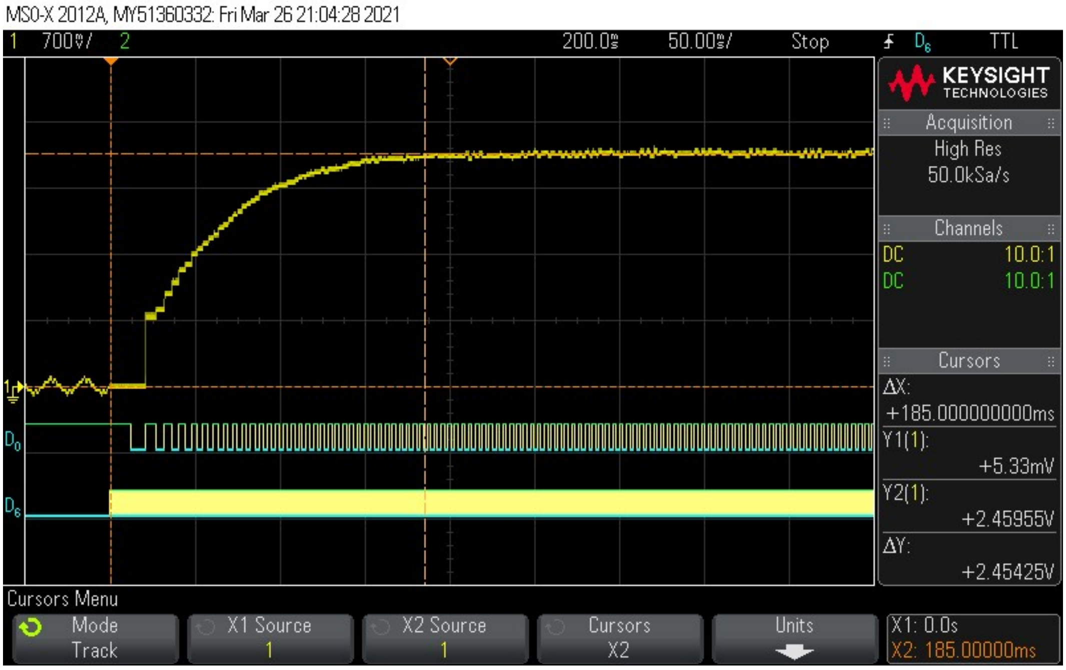

Figure 21. System settling time without PID at target speed 1850 RPM

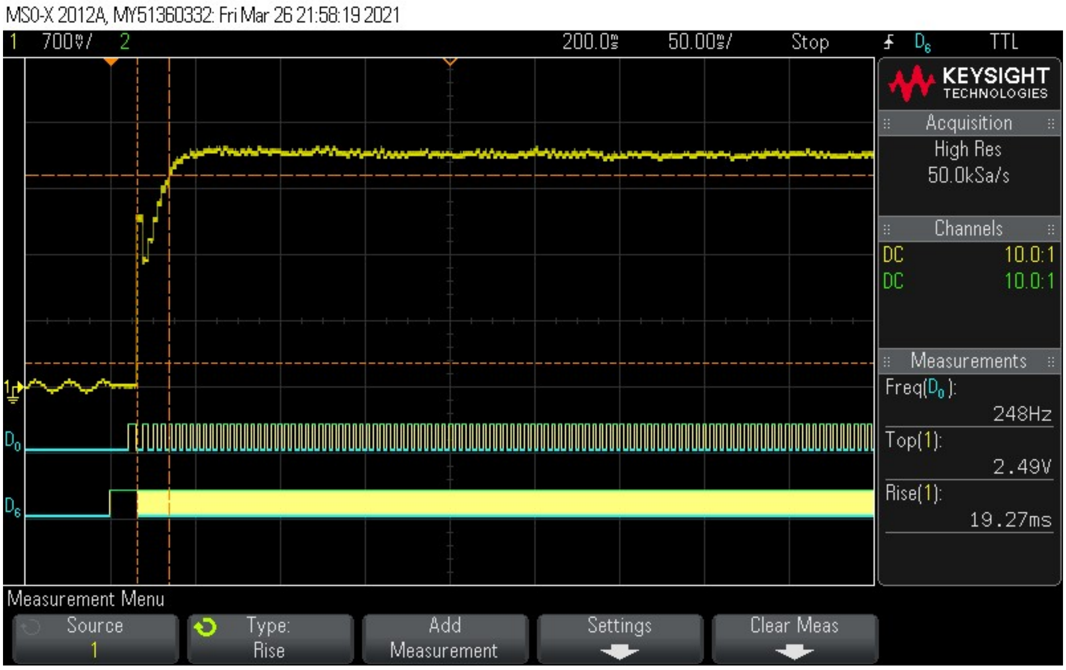

Figure 22. System rise time with PID at target speed 1850 RPM

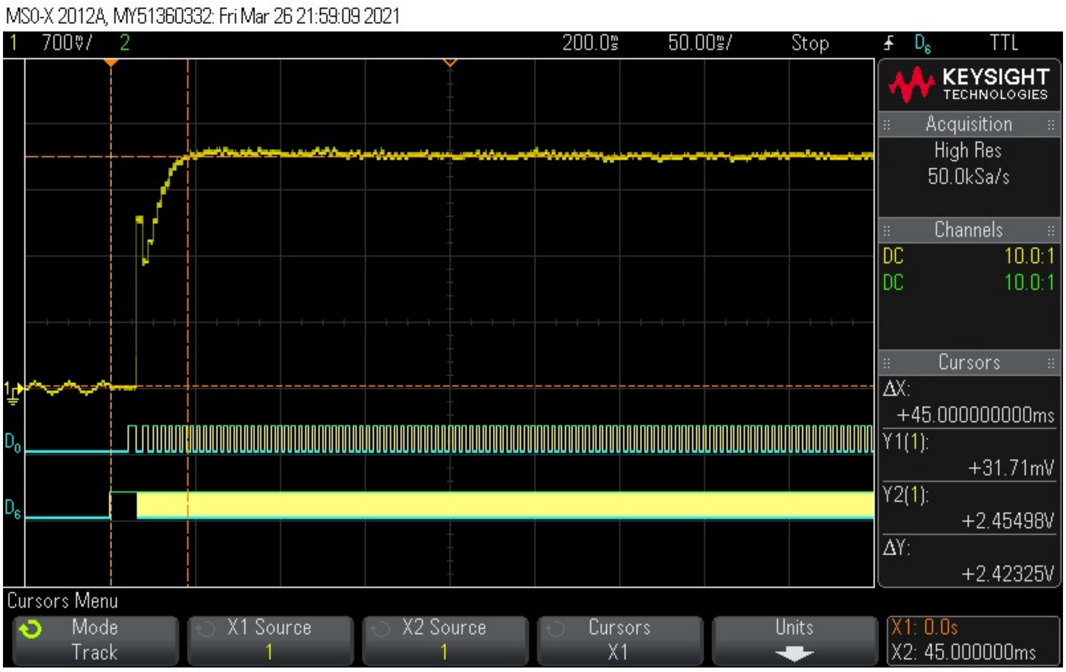

Figure 23. System settling time with PID at target speed 1850 RPM

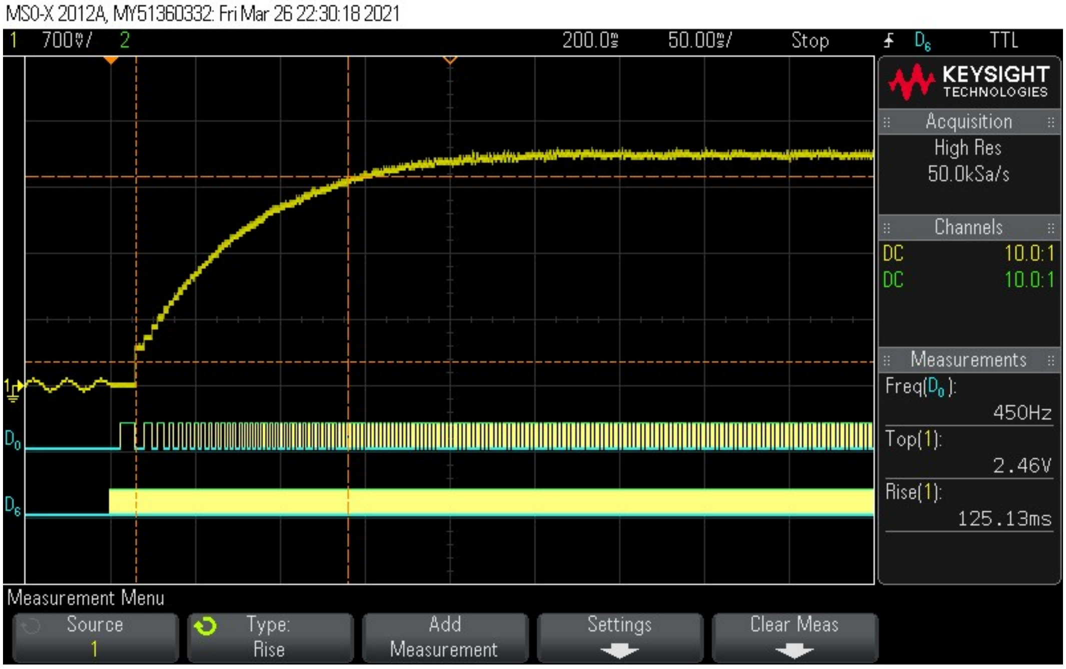

Figure 24. System rise time without PID at target speed 3450 RPM

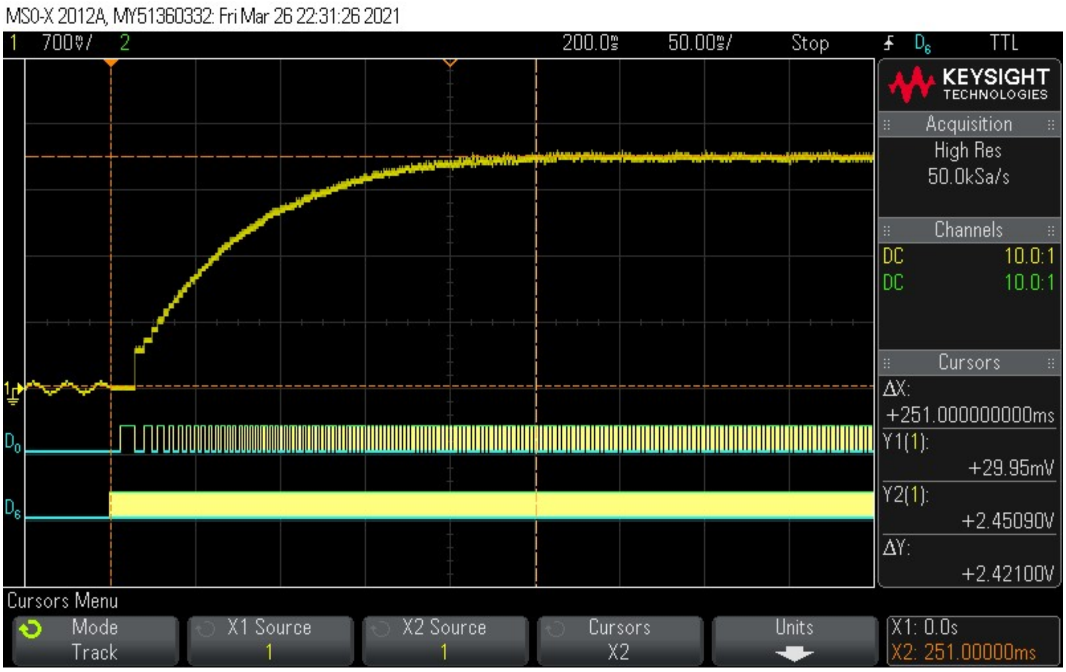

Figure 25. System settling time without PID at target speed 3450 RPM

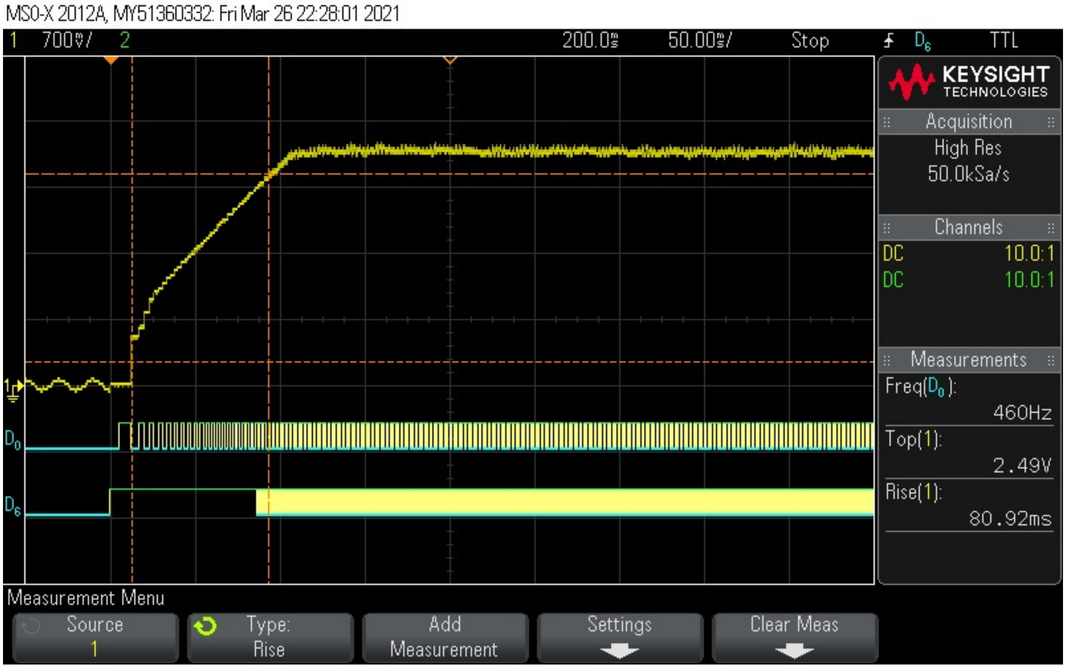

Figure 26. System rise time with PID at target speed 3450 RPM

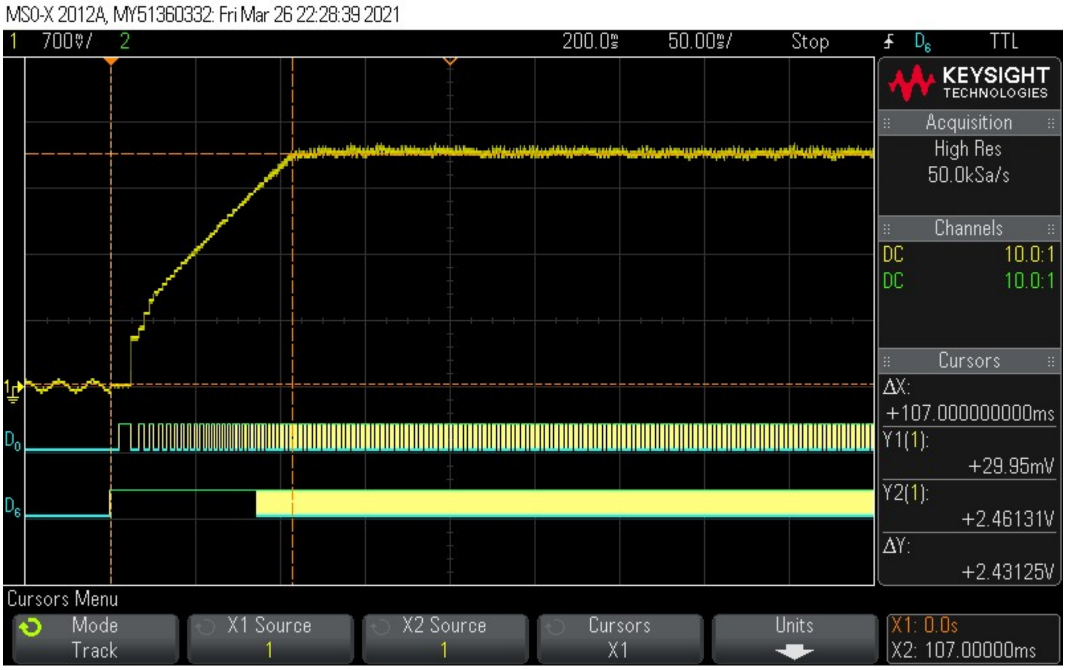

Figure 27. System settling time with PID at target speed 3450 RPM

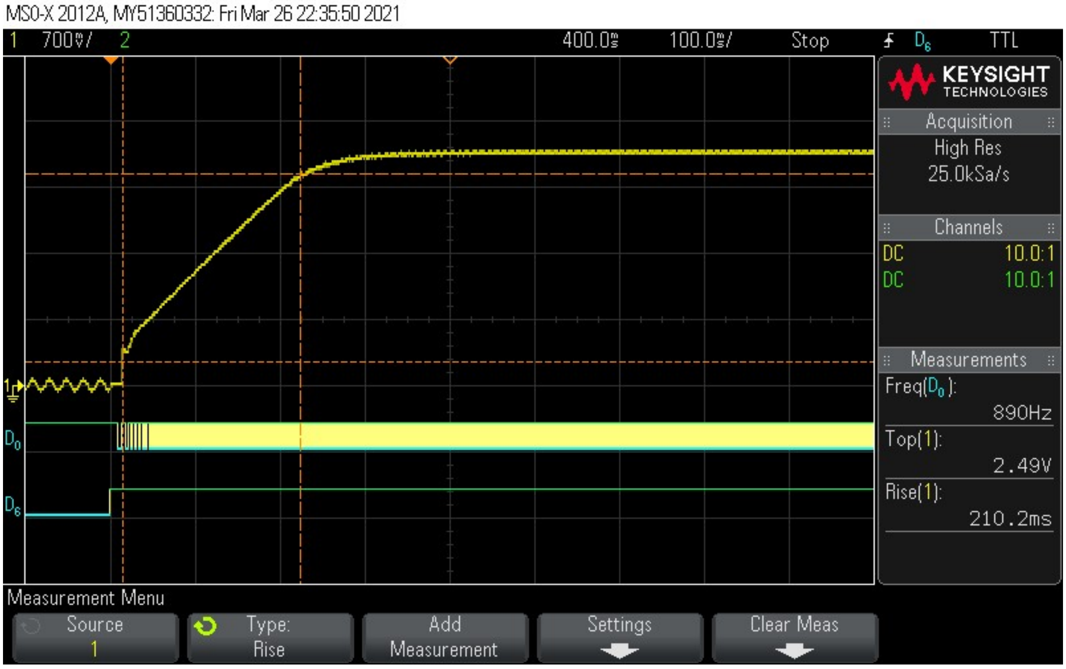

Figure 28. System rise time without PID at target speed 6900 RPM

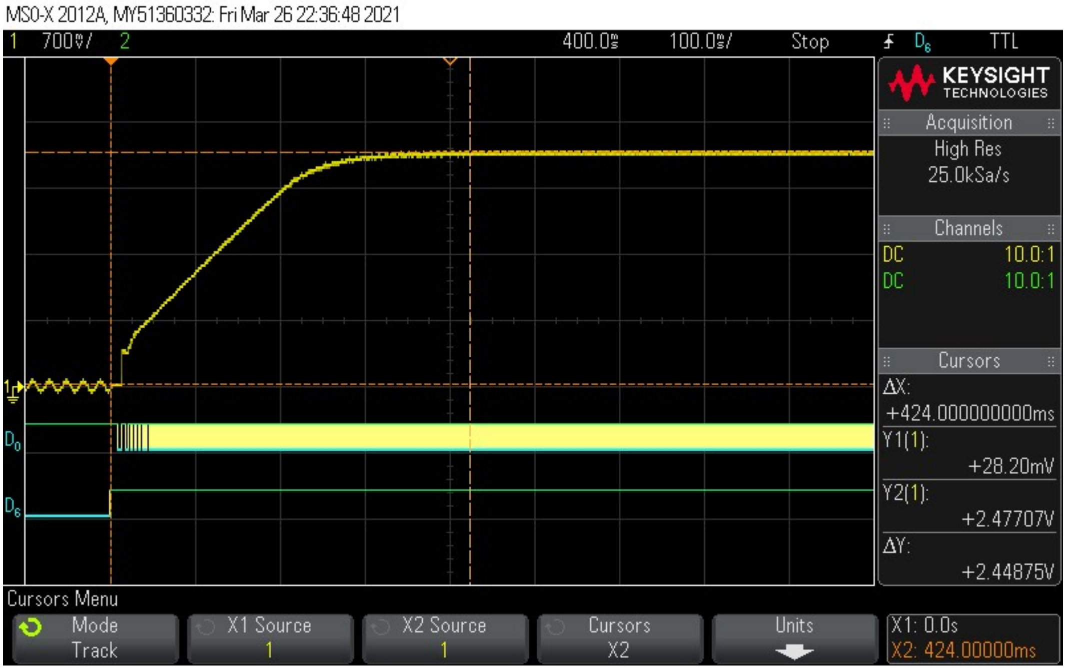

Figure 29. System settling time without PID at target speed 6900 RPM

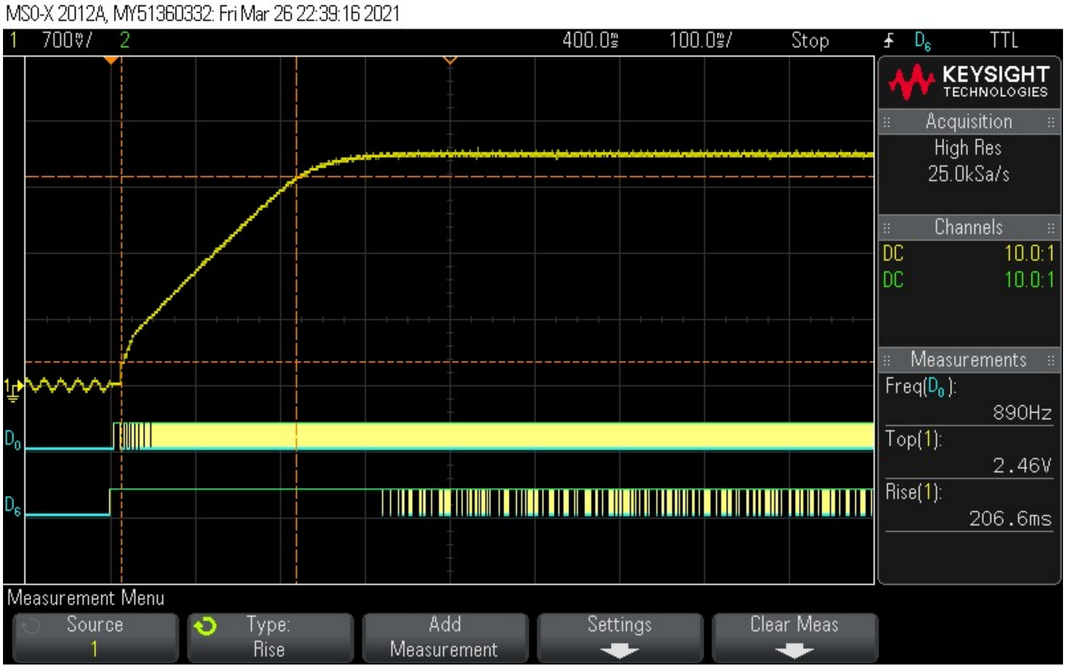

Figure 30. System rise time with PID at target speed 6900 RPM

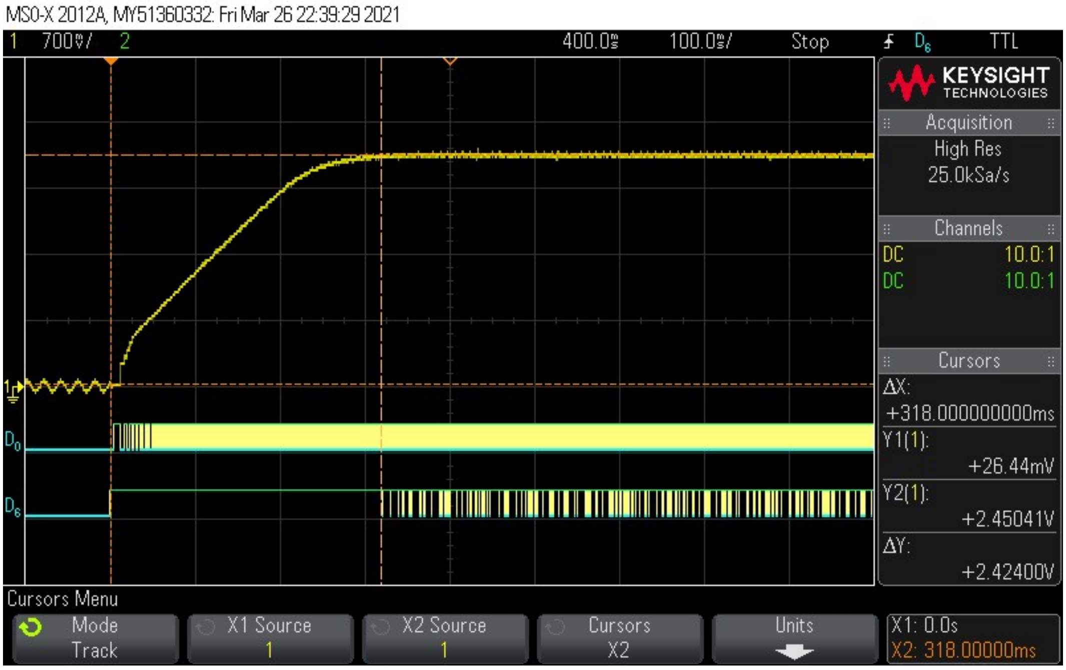

Figure 31. System settling time with PID at target speed 6900 RPM

Table 4. The impact of the PID controller at different target speed

Target speed (RPM)	Rise time (ms)		Settling time (ms)	
	No PID	PID	No PID	PID
1850	88	19	185	45
3450	125	81	251	107
6900	210	207	424	318

For the case of target speed at 1850 RPM, the parameter values for the PID controller were $K_p = 8$, $K_i = 0.15$ and $K_d = 0$. The use of the PID control algorithm significantly reduced the rise time and settling time of the system by more than four times.

At the middle range target speed (at 3450 RPM), the PID controller at first caused an overshoot leading to the need of re-tuning, the new parameter values were $K_p = 8$, $K_i = 0.08$ and $K_d = 0$. The PID controller in this case no longer had such a big impact as in the previous case but was still able to decrease the rise time from 125ms to 81ms (around 150% reduction) and settling time from 251ms to 107ms (about 250% reduction).

At the maximum target speed (6900 RPM), there was barely any difference in the system rise time regardless of the PID controller. This is because the PWM duty cycle and the angular acceleration of the motor had reached the maximum (100% and 45.6 RPM/ms respectively). The settling time was improved at the cost of the system stability; however, this decrease in stability were insignificant.

4 CONCLUSIONS

From measuring results yielded, these following statements were drawn as the conclusion:

- The six-step algorithm was operational as expected.
- The motor speed increased linearly but fluctuated more with increasing PWM values.
- The PID controller eliminated the need of manual control but slightly decreased the system stability.
- Manual tuning method in this project proved to be effective.
- Each range of target speed had a different optimal tuning value for PID parameters.
- The PID controller significantly reduced the motor speed rise time and settling time at a low target speed but had little impact at a high target speed.

In the future, this thesis work can be developed by improving the reusability of six-step module so that it can be used by other microcontrollers and BLDC motors. In addition to that, new software tuning methods are encouraged to be developed to eliminate the need of manual tuning.

REFERENCES

/1/ DC Motor. Wikipedia, 2021. Accessed 18.03.2021. https://en.wikipedia.org/wiki/DC_motor

/2/ Brushless DC Electric Motor. Wikipedia, 2021. Accessed 18.03.2021. https://en.wikipedia.org/wiki/Brushless_DC_electric_motor

/3/ PID Controller. Wikipedia, 2021. Accessed 18.03.2021. https://en.wikipedia.org/wiki/PID_controller

/4/ NUCLEO-L152RE. STMicroelectronics, 2021. Accessed 30.03.2021. https://www.st.com/en/evaluation-tools/nucleo-l152re.html

/5/ X-NUCLEO-IHM07M1. STMicroelectronics, 2021. Accessed 30.03.2021. https://www.st.com/en/ecosystems/x-nucleo-ihm07m1.html

/6/ TrueSTUDIO. STMicroelectronics, 2021. Accessed 30.03.2021. https://www.st.com/en/development-tools/truestudio.html

/7/ UM1943 User Manual. STMicroelectronics, 2015, p4.

/8/ UM1943 User Manual. STMicroelectronics, 2015, p5.

/9/ Fundamentals of Motor Control. STMicroelectronics, n.d., p7.

/10/ Fundamentals of Motor Control. STMicroelectronics, n.d., p20.

/11/ Fundamentals of Motor Control. STMicroelectronics, n.d., p33.

/12/ Fundamentals of Motor Control. STMicroelectronics, n.d., p35.

APPENDIX 1

Motor Speed Result Table

Average values				Sample 1		Sample 2		Sample 3		Sample 4		Sample 5		Sample 6		Sample 7		Sample 8	
PWM val	avg freq	avg speed	error	freq	speed	freq	speed	freq	speed	freq	speed	freq	speed	freq	speed	freq	speed	freq	speed
0	0.0	0	0	0.0	0	0.0	0	0.0	0	0.0	0	0.0	0	0.0	0	0.0	0	0.0	0
500	34.7	261	8	35.4	265	33.7	252	35.1	263	35.5	266	34.5	259	33.8	254	35.1	264	34.9	262
1000	60.1	451	7	60.2	452	59.2	444	60.1	451	60.4	453	60.3	452	60.3	452	60.2	452	60.1	450
1500	113.4	851	6	113.4	851	113.6	852	113.6	852	113.4	850	112.6	844	113.5	851	113.1	848	114.0	855
2000	175.2	1314	11	174.8	1311	176.0	1320	176.6	1325	174.8	1311	174.2	1307	173.9	1304	175.6	1317	175.9	1319
2500	216.6	1624	12	216.3	1622	215.2	1614	215.5	1616	216.3	1622	217.0	1628	217.4	1631	218.2	1637	216.6	1625
3000	254.1	1905	12	253.6	1902	253.9	1904	253.3	1900	255.6	1917	254.1	1906	254.3	1907	254.2	1907	253.4	1901
3500	291.1	2183	11	290.5	2179	292.1	2191	291.6	2187	292.6	2195	290.4	2178	290.2	2177	290.2	2177	291.0	2183
4000	345.0	2587	21	344.6	2585	346.1	2596	342.9	2572	343.0	2573	344.6	2585	347.8	2609	345.3	2590	345.3	2590
4500	394.1	2956	17	394.6	2960	395.3	2965	395.7	2968	394.6	2960	392.2	2942	393.6	2952	391.9	2939	395.1	2963
5000	457.7	3433	18	457.9	3434	457.0	3428	455.4	3416	457.5	3431	456.2	3422	459.6	3447	458.7	3440	459.6	3447
5500	484.8	3636	24	483.0	3623	485.0	3638	484.0	3630	482.0	3615	485.0	3638	485.0	3638	486.0	3645	488.0	3660
6000	532.4	3993	33	530.2	3977	534.2	4007	534.8	4011	534.8	4011	534.8	4011	530.8	3981	528.0	3960	531.9	3989
6500	589.5	4422	21	591.7	4438	586.9	4402	591.7	4438	586.9	4402	588.2	4412	588.2	4412	592.4	4443	590.3	4427
7000	627.4	4705	30	630.0	4725	627.5	4706	628.8	4716	628.5	4714	625.9	4694	623.4	4676	628.1	4711	626.9	4702
7500	672.1	5041	37	672.0	5040	670.6	5030	672.0	5040	673.1	5048	677.1	5078	671.0	5033	672.0	5040	669.2	5019
8000	710.3	5327	35	705.6	5292	713.4	5351	708.5	5314	713.1	5348	711.8	5339	712.8	5346	706.5	5299	710.8	5331
8500	750.4	5628	32	751.0	5633	749.2	5619	754.6	5660	750.8	5631	746.1	5596	748.7	5615	749.2	5619	753.5	5651
9000	799.3	5995	27	801.5	6011	799.7	5998	800.8	6006	801.3	6010	799.2	5994	795.7	5968	799.5	5996	796.9	5977
9500	877.3	6580	37	874.4	6558	879.7	6598	877.8	6584	878.7	6590	880.0	6600	877.5	6581	872.3	6542	877.8	6584
10000	915.5	6866	33	915.8	6869	917.8	6884	917.8	6884	915.1	6863	911.1	6833	915.8	6869	912.4	6843	918.4	6888

APPENDIX 2

D6230 Three-phase BLDC Motor Driver Schematic

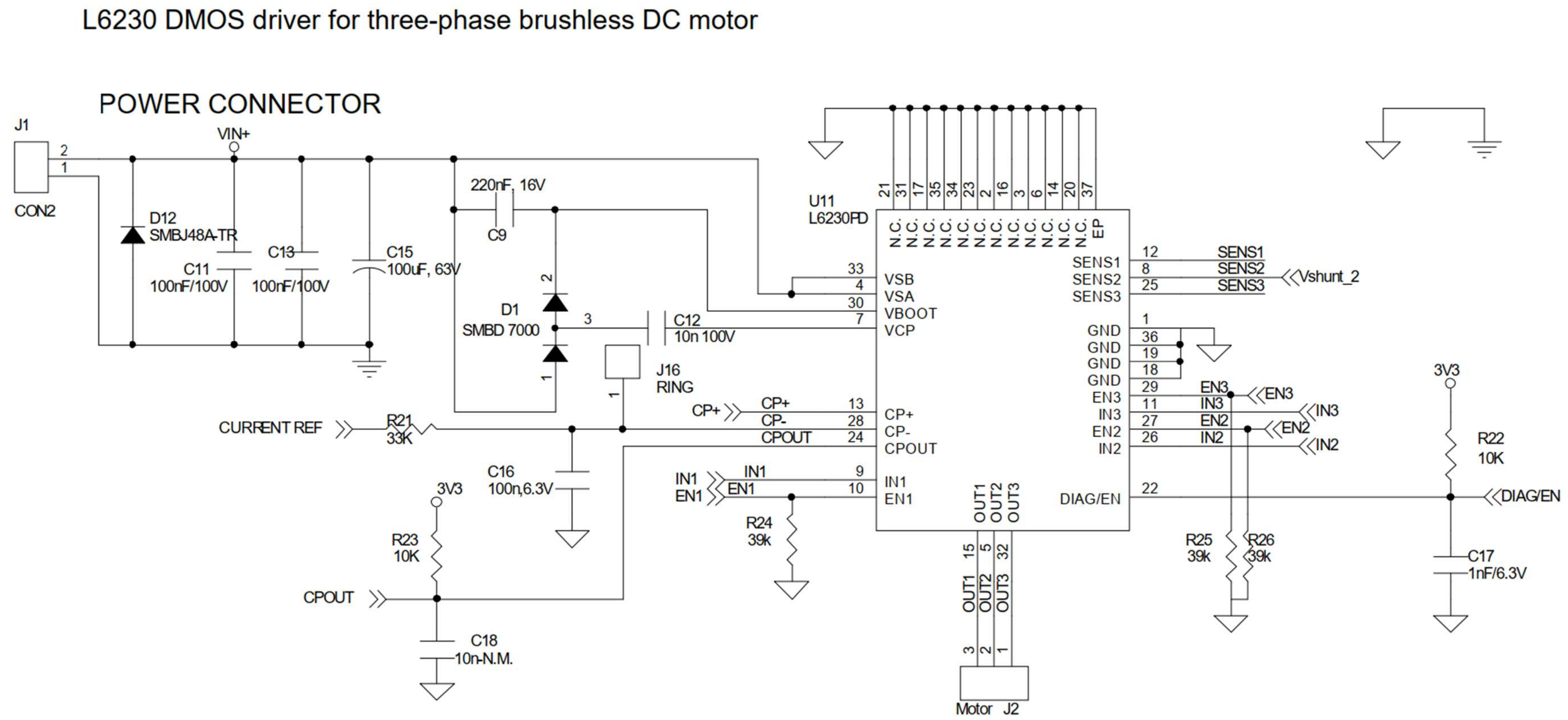

APPENDIX 3

Hall Sensor Schematic